Design and Characterization of a 3D Superconducting Architecture for Fast Readout and Remote Entanglement

Nick Schwegler
ETH Zürich
Semester Thesis

Supervisors:
Philipp Kurpiers
Prof. Dr. Andreas Wallraff

April 8, 2018

Abstract

One possibility of a scalable architecture for superconducting quantum bits (qubits) is based on distributive quantum information processing. It requires connecting distant quantum nodes with classical and quantum channels to build a quantum network. In order to achieve high entangling rates for distributed quantum computing, a direct quantum channel which realizes deterministic remote entanglement with high fidelity between different nodes is necessary [1, 2, 3].

This project describes the design, simulation and realization of 3D cavities forming the basis of a quantum node. By incorporating 3D cavities into the design it is possible to realize a direct connection to a microwave waveguide. This enables a quantum channel with minimal loss. Additionally, a coupling of two 3D cavities realizes a Purcell filter, which is advantageous fast readout [4]. Furthermore, superconducting qubits in 3D designs typically achieve increased life- and coherence times compared to 2D implementations [2].

Contents

1 Introduction **3**

2 Design Criteria **4**
2.1 Waveguide 4
2.2 PF and QB Cavity 4
2.3 Qubit Placement 7
2.4 Coupling 7
2.4.1 Coupling PF cavity to outside ports 7
2.4.2 Coupling PF cavity to QB cavity 7
2.4.3 Coupling QB cavity to waveguide 7
2.5 Frequency Tunability 8

3 Simulations **8**
3.1 Coupling 8
3.1.1 Coupling PF cavity to outside ports 8
3.1.2 Coupling PF cavity to QB cavity 9
3.1.3 Coupling QB cavity to waveguide 10
3.2 Surface Currents 14
3.3 Manufacturing Tolerances and Frequency Tunability 14

4 Realization **17**
4.1 PF and QB cavity 17
4.2 Coupling 18
4.3 Waveguide 18
4.4 Frequency Tunability 18
4.5 Thermalisation 18

5 Experimental Results **18**
5.1 Discussion of Experimental Results 19

References **21**

A Qubit Lifetime Simulation **24**
A.1 Theory 24
A.1.1 Approach A 24
A.1.2 Approach B 24
A.2 Simulation 25
A.3 Conclusion 26

1 Introduction

This semester thesis discusses the design, simulation and realization of two 3D cavities directly coupled to each other. In addition, one of the cavities is coupled to coaxial cables for readout and the other one to a waveguide for quantum communication. A schematic of the final device is shown in Fig. 1.

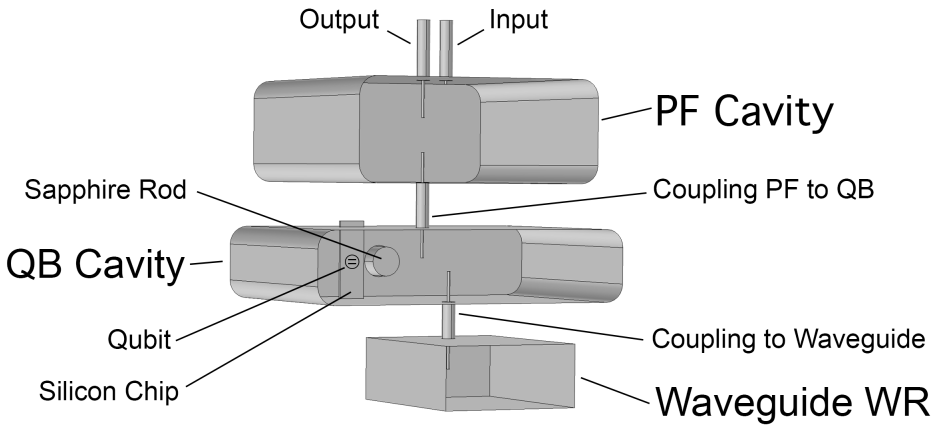

Figure 1: Interior boundaries of the final design as modelled in COMSOL. The two front facing cavity boundaries are removed for visibility. The bottom cavity (QB) contains the qubit on a silicon chip, the top cavity (PF) acts as the Purcell filter. The connection to the outside is done using the output and input ports (coaxial cables) at the top. The bottom QB cavity is tuneable via insertion of a sapphire rod. At the bottom, the waveguide (WR90) acts as a quantum channel connecting two nodes. The coupling between the cavities and to the waveguide are realized by antennas.

A good characterization of the control over a quantum network is the demonstration of the violation of a Bell inequality [5, 6, 7]. This Bell test can be used as a witness for entanglement. In addition it shows the existence of a non-local interaction, if the experiment is performed without loopholes. A loophole-free Bell test using typical circuit QED systems requires the two quantum nodes to be spatially separated over tens of meters. The device designed in this project is planned to be used for a Bell test in the future.

2 Design Criteria

In the following section the main design criteria for the device are described in detail. The final technical drawings are shown in appendix B.

2.1 Waveguide

The unidirectional coherent interaction required for the generation of deterministic remote entanglement is mediated by microwave photons [8, 9]. Rectangular waveguides represent an efficient way of transmitting microwave photons over distances of tens of meters [10]. Low loss in a 3D architecture is obtained by direct coupling of the QB cavity to the rectangular waveguide.

In addition, rectangular waveguides have a cut-off frequency f_C, suppressing the propagation of modes below f_C exponentially. The waveguide used in this setup (WR-90) has an operating range from 8.3 to 11 GHz and a cut-off frequency $f_C = 6.5$ GHz.

2.2 PF and QB Cavity

The transmon qubit should be fabricated on a silicon chip and placed into the QB cavity. The Purcell filter (PF) is coupled to the QB cavity. The QB cavity couples trough the Purcell filter to an external transmission line. This enables the selection of particular modes that couple to the outside. Only modes that are also supported in the PF cavity can decay from the QB cavity.

Without the Purcell filter, the output port would be placed at the QB cavity, coupling the environment directly to multiple modes of the cavity. The Purcell filter reduces the number of available modes. The suppression of modes at the qubit frequency reduces the qubit decay via this decay channel. The qubit lifetime can therefore be increased beyond the limit imposed by the bandwidth of the QB cavity modes through the Purcell effect.

As a consequence, the Purcell filter allows for fast readout, since the readout time decreases with stronger coupling of the qubit to the cavity mode and the effective linewidth of the cavity.

There are three relevant frequencies for the cavity design:

$f_{\text{Readout}} = 4.8$ GHz: This frequency is used for the dispersive readout of the qubit. It is an eigenfrequency of both the QB and PF cavity.

$f_{\text{Qubit}} = 6.3$ GHz: This is the transition frequency from the ground state to the first excited state of the transmon qubit. To guarantee a long lifetime, this frequency is not resonant with any modes of the QB and PF cavity.

$f_{\text{Transfer}} = 8.35$ GHz: At this frequency, the quantum communication between the two nodes is realized. This frequency is an eigenmode of the QB cavity only.

The cut-off frequency f_C of the waveguide is such that

$$f_{\text{Readout}}, f_{\text{Qubit}} < f_C < f_{\text{Transfer}}. \tag{1}$$

The eigenfrequencies of a rectangular cavity of size $(a \times b \times d)$ are given by

$$f_{mnl} = \frac{c}{2\pi\sqrt{\mu_r \epsilon_r}} \sqrt{\left(\frac{m\pi}{a}\right)^2 + \left(\frac{n\pi}{b}\right)^2 + \left(\frac{l\pi}{d}\right)^2}, \tag{2}$$

where c is the speed of light, μ_r the permeability, ϵ_r the permittivity and m, n, l integers.

We are only interested in the lowest eigenmodes, which have n = 0, hence they do not depend on the height of the cavity, leaving us with two parameters per cavity $(a \times d)$. The heights of the two cavities are chosen as small as possible such that the coupling pins fit inside and such that modes with n > 0 are at frequency higher than $f_{111} = 13.4$ GHz. In particular b = 12 mm for the QB and b = 17 mm for the PF cavity.

The only condition for the PF cavity is that $f_{101} = f_{\text{Readout}}$. To reduce the amount of different eigenfrequencies, the PF cavity is chosen to be quadratic. This results in a rectangular cavity of approximately 43×43 mm.

The QB cavity has two conditions: $f_{101} = f_{\text{Readout}}$ and $f_{102} = f_{\text{Transfer}}$. This requires a rectangular cavity of approximately 55.2×36.4 mm.

These four dimensions already give the complete mode structure as seen in Fig. 2.

Note that from these particular mode design criteria, the QB cavity has an unwanted mode at $f_{201} = 6.75$ GHz. However, the qubit does not strongly couple to this mode due to its placement (see next section). This mode also has a high Q value, because neither the PF cavity nor the waveguide couple to this mode.

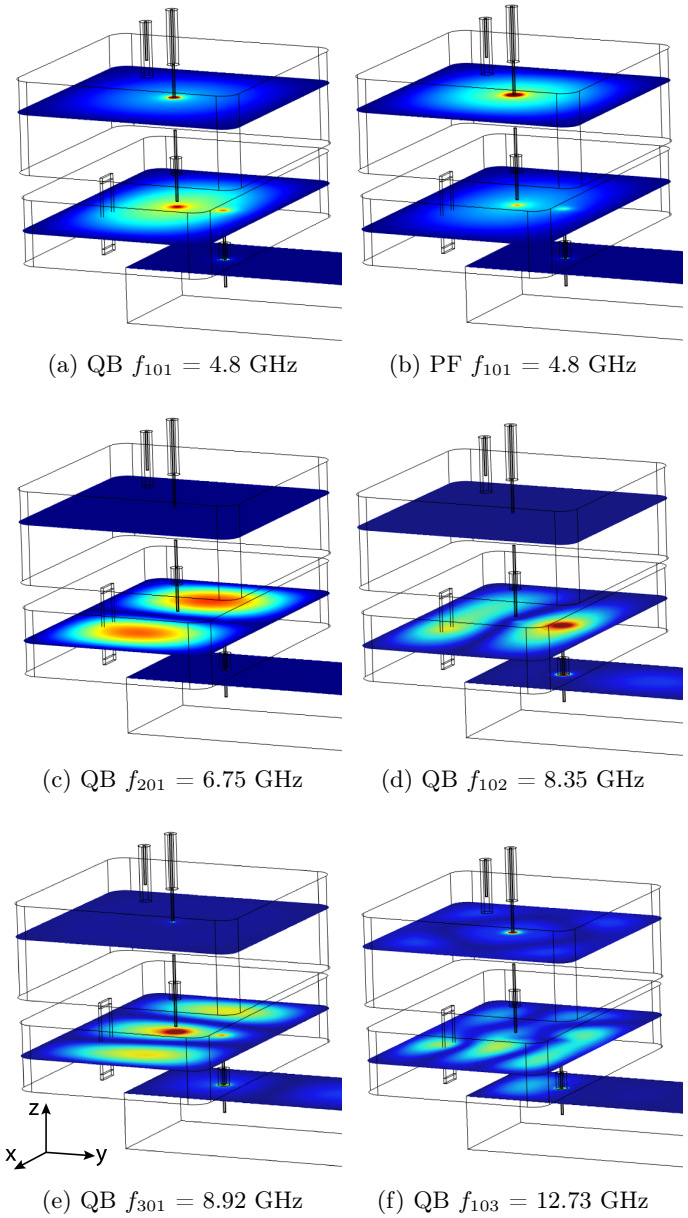

(a) QB $f_{101} = 4.8$ GHz (b) PF $f_{101} = 4.8$ GHz

(c) QB $f_{201} = 6.75$ GHz (d) QB $f_{102} = 8.35$ GHz

(e) QB $f_{301} = 8.92$ GHz (f) QB $f_{103} = 12.73$ GHz

Figure 2: The norm of the electric field for three planes is plotted in color, where red is high and dark blue is low. The black outlines represent the boundaries of the device, which shows the same features as in Fig. 1, without the sapphire rod. Shown are some selected eigenmodes of the PF (top) and QB (bottom) cavity. On the bottom, the modes inside the waveguide (WR) are also shown. The eigenmodes are simulated in COMSOL.

2.3 Qubit Placement

The transmon qubit is placed inside the QB cavity on top of a silicon chip, as seen in Fig. 2. We require the qubit to only couple to the 101 and 102 mode.

By placing the qubit at (d/4, a/3) in the x-y plane, the coupling to the first two unwanted modes (201 and 301) is minimized. The first higher mode that couples to the qubit and the waveguide is the mode at $f_{103} = 12.73$ GHz.

2.4 Coupling

All couplings are realized with coaxial cables, which form an antenna coupling through an exposed centre conductor pin. The pin length determines the strength of the coupling. With the position of the pins, the eigenmodes that will be coupled can be selected. In combination with the discrete eigenmode spectrum of 3D cavities, this allows for precise control of the coupling between cavities, to waveguides or to the outside.

2.4.1 Coupling PF cavity to outside ports

The input and output ports are placed on top of the PF cavity. The readout is performed at $f_{\text{Readout}} = f_{101} = 4.8$ GHz. The output port is thus placed at the maximum of the 101 mode, which is the middle. As a compromise, the input port is displaced from the middle by 1.5 mm. Since the input port is around 100 times weaker coupled than the output port, the broken symmetry should have a reduced effect.

2.4.2 Coupling PF cavity to QB cavity

We want to exclusively Purcell filter the 101 mode, thus only this mode should be coupled between the PF and QB cavity. The coupling pins are placed in the middle of both cavities, which is the maximum of the 101 mode. This mode is the only relevant Purcell filtered mode. Higher eigenmodes are either not coupled due to the pin placement, never resonant for both cavities such that excitations can not transfer between the QB and PF cavity, or are far detuned from the qubit frequency. This should prevent the qubit from decaying to the PF cavity.

2.4.3 Coupling QB cavity to waveguide

The coupling between the QB cavity and the waveguide is also realized by an antenna. A hole aperture could not achieve a strong enough coupling on the

order of tens of MHz. The waveguide is required to couple to the 102 mode of the QB cavity. Hence the coupling pin inside the QB cavity is placed at the maximum of the 102 mode at (d/4, a/2) in the x-y plane.

2.5 Frequency Tunability

An interaction between two separate nodes requires the transfer mode $f_{\text{Transfer}} = f_{102}$ to be on resonance. However, due to manufacturing limitations, we expect uncertainties in the cavity modes, see section 3.3. Thus the ability to tune the 102 mode of the QB cavity of at least one of the two nodes is necessary. By tuning the 102 mode of the QB cavity of one node, its 101 mode is also shifted and no longer on resonance with the 101 mode of the connected PF cavity. The resulting detuning needs to be corrected by reworking the corresponding PF cavity. The tunability is realized by inserting a sapphire rod into one side of the QB cavity at the maximum of the 102 mode at (b/2, a/2) in the x-z plane.

3 Simulations

All of the simulations are done in COMSOL Multiphysics 5.1, using the eigenfrequency and frequency domain solver of the RF module.

3.1 Coupling

3.1.1 Coupling PF cavity to outside ports

The coupling κ of the input and output ports at the PF cavity can be determined directly from the quality factor Q simulated with the eigenfrequency solver. It is given by the relation

$$\frac{\kappa}{2\pi} = \frac{\omega}{Q}. \tag{3}$$

The output port couples with $\kappa_{\text{out}}/2\pi = 48$ MHz to the 101 mode for a pin length of 6.2 mm. The input port couples with $\kappa_{\text{in}}/2\pi = 730$ KHz to the 101 mode for a pin length of 0.6 mm. Due to its displacement, the input port also couples weakly to the 102 and 201 modes. This coupling is of order 80 KHz, so 10 times weaker than the coupling to the 101 mode.

3.1.2 Coupling PF cavity to QB cavity

A transmission measurement from the input port 1 to the output port 2 (at the PF cavity) allows to evaluate the coupling between the PF and QB cavity. In Fig. 3, the simulated S_{21}-parameter is fitted with a model for coupled cavity systems [11]. To obtain a coupling strength of 10.9 MHz, a pin length of 5 mm reaching into each cavity is necessary. The PF cavity has an eigenfrequency of $f_{101} = 4.834$ GHz, where as the QB cavity has $f_{101} = 4.848$ GHz.

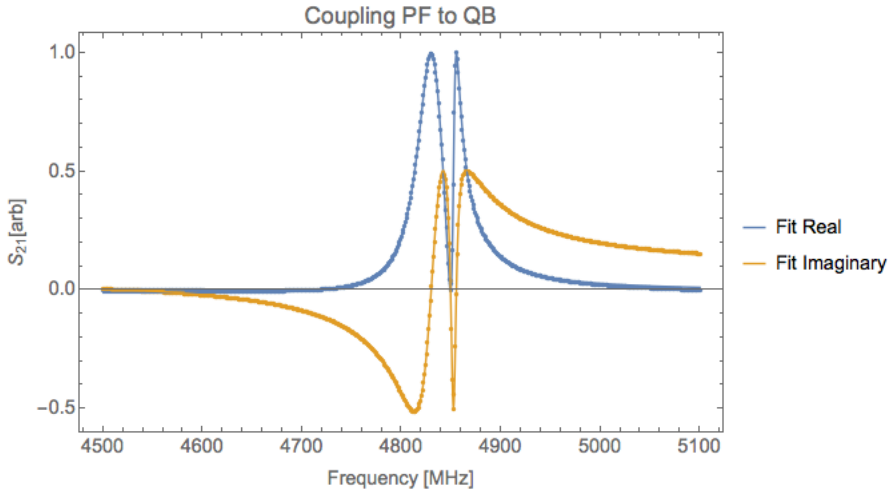

Figure 3: Real and imaginary part of simulated S_{21}-Parameter (points), fitted with a model for coupled cavity systems (line). Port 1 is the input at the PF cavity, port 2 the output.

From the electric field distribution, we also observe a distortion of the eigenmodes due to the deviation in permittivity induced by the sapphire chip, which brakes the symmetry. The 201 mode is quenched and its anti-node is shifted from the middle. To minimize the coupling of this mode to the PF cavity, the pin inside the QB cavity is displaced by 0.5 mm from the middle by shifting the whole bottom QB cavity with respect to the PF cavity. In Fig. 4, the transmission from the input port 1 at the PF cavity to an extra output port 4 at the QB cavity is simulated. Without the displacement described above, the resonance at 6.75 GHz couples stronger to the environment. With a displacement of 0.5 mm, the resonance of the 201 mode shows a high Q value, indicating the reduced coupling to the output coaxial wire. The resonance can be further suppressed by placing another

silicon chip into the QB cavity on the opposite side to restore the symmetry. We have not done this to keep construction simple.

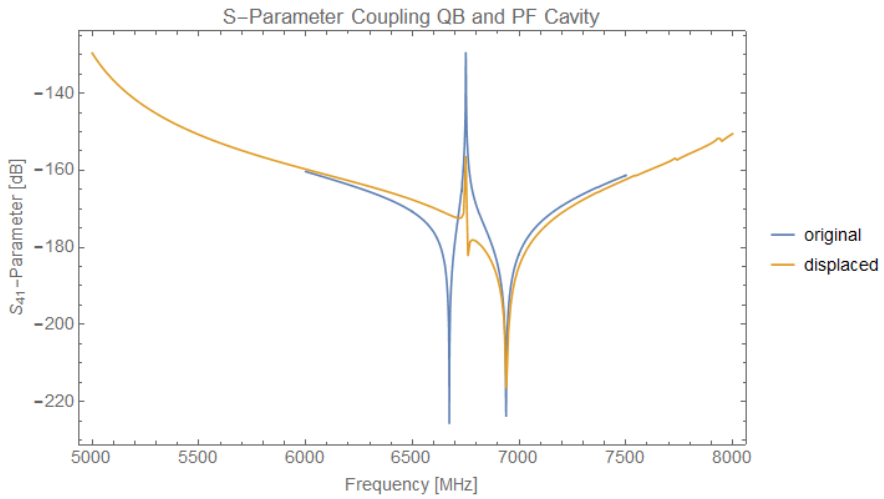

Figure 4: Simulated S_{41}-Parameter of the 201 QB cavity mode. Port 1 is a coaxial port at the PF cavity, Port 4 at the QB cavity.

3.1.3 Coupling QB cavity to waveguide

The coaxial pin inside the waveguide represents a right-angle coax to waveguide transition. This connection has two parameters: The pin length reaching into the waveguide and the distance of the pin to the end on the waveguide, which is called back-short. In Fig. 6 the S-parameters of a coaxial input port C placed on top of a WR90 rectangular waveguide (without QB / PF cavity) to a rectangular output port W are simulated. The two parameters are optimized to minimize the reflection at the transfer frequency f_{Transfer}. The resulting pin length is 7.05 mm and the back-short 7.4 mm. Below the cut-off frequency of around 6.5 GHz, the propagation of modes in the waveguide is exponentially suppressed, thus $S_{WC} \to -\infty$ dB, while $S_{CC} \to 0$ dB. At $f_{\text{Transfer}} = 8.35$ GHz the reflection is maximally suppressed: $S_{WC} = -0.16$ dB and $S_{CC} = -38$ dB.

This represents an infinite coaxial cable coupling to the waveguide. However in our setup, we want to couple the 102 QB cavity mode to the waveguide. Hence, the optimal pin length for our coupling differs from the one found above. For a coupling of 18 MHz at a frequency of 8.359 GHz a pin length of 4.8 mm reaching into the waveguide is needed. The pin length inside

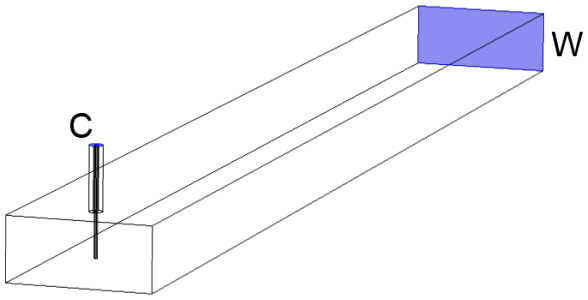

Figure 5: COMSOL model of the boundaries used for the simulation of the coupling between the coaxial cable and the waveguide. The two ports are marked in blue: Coaxial cable port C on top of the waveguide, and rectangular waveguide port W at the back.

the QB cavity is 4.4 mm. This coupling can be evaluated from a reflection measurement on the rectangular port 3. The simulated S_{33}-parameter can be found in Fig. 7.

From the same simulation, the absolute values squared of all S-parameters are shown in Fig. 8. This reveals that all of the lost signal exits at the output port at the PF cavity. The loss is about 0.8 %.

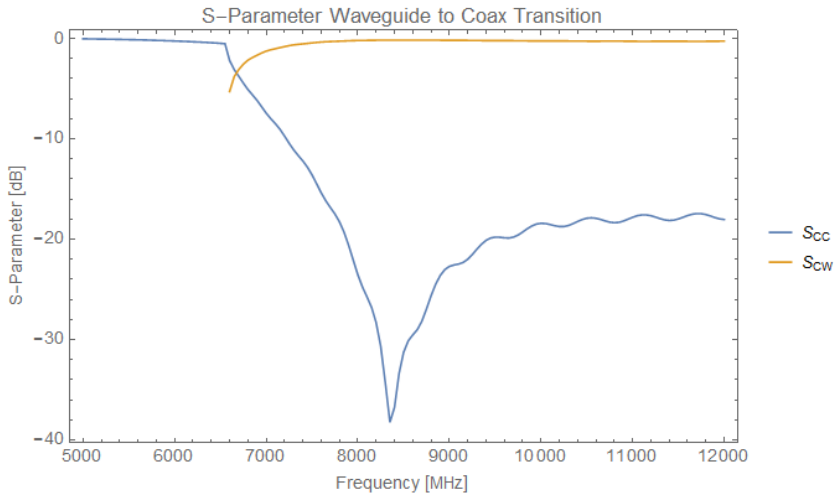

Figure 6: Simulated reflection and transmission S-Parameter of a coax to waveguide transition. Port C is the coaxial cable coming from the QB cavity, Port W the rectangular waveguide.

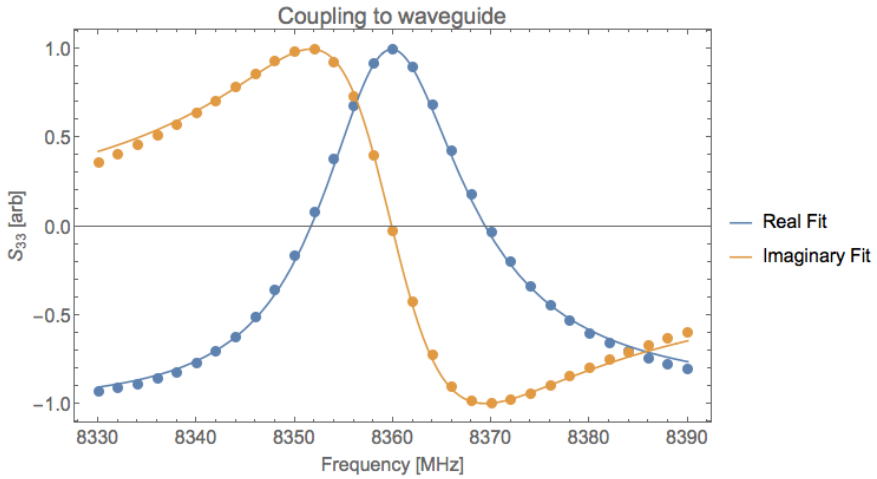

Figure 7: Real and imaginary part of simulated S_{33}-Parameter (points) of the waveguide coupled to the QB cavity, fitted with a complex Lorentzian (line). Port 3 is the rectangular port at the waveguide.

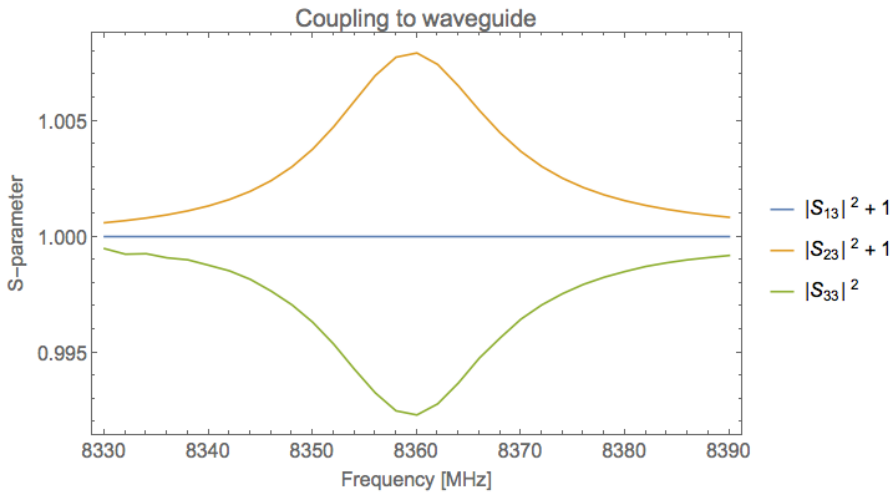

Figure 8: Simulated S-Parameter of the waveguide coupled to the QB cavity. Port 1 and 2 are coaxial output ports at the PF cavity and Port 3 is the rectangular input port at the waveguide.

3.2 Surface Currents

The surface currents of the two cavities go along the z direction, as seen in Fig. 9. Due to manufacturing constraints, each cavity needs to be made out of two pieces. In order to minimize current loss, the cavities are separated along the the current direction.

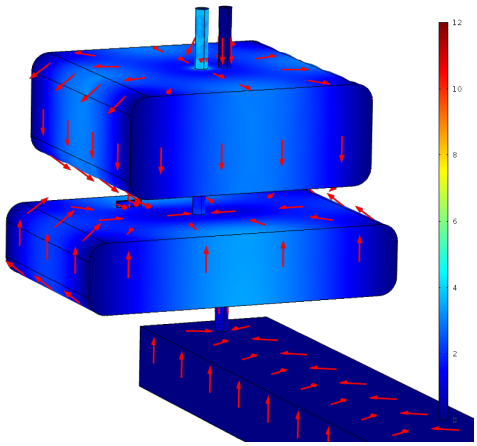

Figure 9: Simulation of the normalized surface current density (red arrows) and its norm (color boundaries, in A/m) for f_{Readout}. The surface currents go along the z direction of the two cavities. The device shows the same features as Fig. 1.

3.3 Manufacturing Tolerances and Frequency Tunability

The deviation of the cavity eigenfrequencies due to manufacturing limitations is estimated by incorporating tolerances into all cavity dimensions when simulating the eigenmodes. Assuming tolerances of 0.5 mm, in the worst case we expect to observe shifts in the eigenfrequencies of 8 MHz.

Two options to correct for the expected shift in eigenfrequency of the 102 mode of the QB cavity are considered, both involve the precise insertion of a rod of different material through a hole in the side of the QB cavity.

The first option is a rod made out of a conductive material, e.g. aluminium. Essentially this represents a very bad coaxial port with a highly mismatched impedance, thus the loss of electric field is minimal. This is achieved by making the gap between the rod and the cavity as small as possible without touching.

The second material is a dielectric, e.g. sapphire. The loss through the hole in this case is suppressed by a high cut-off frequency, which is 35 GHz for a hole of 5 mm diameter.

The simulated shift in eigenfrequency $\Delta f_{nml}(x)$ of the mode nml depending on the insertion length x of the two possible rods are shown in Fig. 11 and 10. The conductive rod first introduces a shift in positive direction relative to zero insertion, then changes direction at a certain insertion length. The dielectric rod introduces a negative shift. For both options the 102 eigenmode with initial frequency f_{Transfer} is influenced the most, with $\Delta f_{102}(4\text{ mm}) \approx 30$ MHz.

Due to the cavity mode structure, other modes than the 102 mode are also affected by the tuning. A compromise has to be made, and a slight shift in frequency f_{Readout} of the 101 mode needs to be accepted. The difference between the two options becomes apparent for this 101 mode. The conductive rod induces a bigger shift ($\Delta f_{101}(4\text{ mm}) \approx 20$ MHz) compared to the dielectric rod ($\Delta f_{101}(4\text{ mm}) \approx 4$ MHz). Due to the coaxial nature of the first option, there are also new dipole modes introduced, and most eigenmodes are deformed. For these reasons using a sapphire rod is advantageous.

In Fig. 11 we observe $\Delta f_{102}(4\text{ mm}) - \Delta \text{f}_{102}(1\text{ mm}) \approx 30$ MHz with 3 mm travel. At $x_0 = 3$ mm insertion we observe $\Delta f_{102}(x_0) \approx 15$ MHz. The QB cavity is fine tuned, i.e. shortened by 0.14 mm in both length and width in order to bring frequency $f_{\text{Transfer}} = f_{102}(x_0)$ to this half point. This gives the ability to adjust f_{Transfer} for 15 MHz in both directions with 3 mm travel compared to the fixed cavity.

To bring the 101 mode of the QB and PF cavity back into resonance, the PF cavity is shortened by 0.1 mm in length and width such that $f_{101}^{PF} = f_{101}^{QB}(x_0)$.

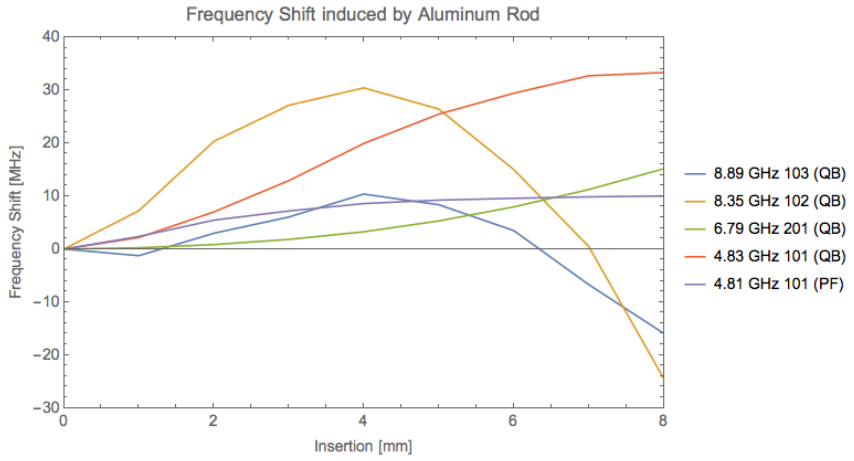

Figure 10: Simulated shift in frequency of the QB cavity induced by the insertion of an aluminium rod of 5 mm diameter. The shift is relative to the frequency at zero insertion and plotted for selected eigenmodes.

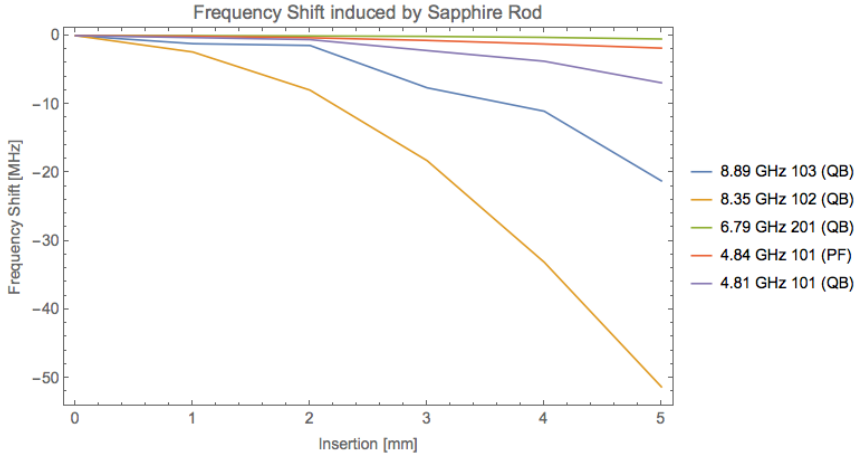

Figure 11: Simulated shift in frequency of the QB cavity induced by the insertion of a sapphire rod of 5 mm diameter. The shift is relative to the frequency at zero insertion and plotted for selected eigenmodes.

4 Realization

This section describes the realization of the cavity system discussed above. All components are designed in Autodesk Inventor. Two designs are finalized: One tuneable in frequency, the other one fixed.

The final fixed device consists of four elements: Waveguide Connector, Cavity Main, PF Cavity Lid and QB Cavity Lid. For the tuneable device, the QB Cavity Lid is altered, and a Translation Stage is added.

An exploded view of the final tuneable device can be seen in Fig. 12. All elements are milled in aluminium 6061, except for the Translation Stage, which is made out of copper.

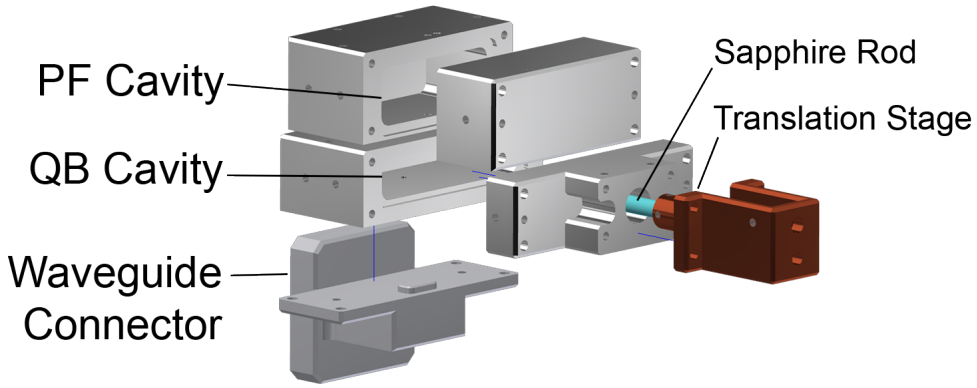

Figure 12: Exploded view of the final tuneable device rendered in Autodesk Inventor. Components from bottom left to right: Waveguide Connector, Cavity Left, PF Cavity Right, QB Cavity Right, Sapphire Rod, Translation Stage.

4.1 PF and QB cavity

The PF and QB cavity are made out of three parts in total. Cavity Main is the main part into which the QB and PF cavity are milled. This part defines the position of the cavities with respect to each other. Each cavity is closed with a lid (QB Cavity Lid and PF Cavity Lid) which is attached with M3 screws. A centring on each cavity guarantees a precise fit. The QB cavity is separated at the qubit position, such that the sapphire chip can be placed into a milled holder.

4.2 Coupling

All coaxial cables are hold in place by M2 grub screws, which are placed in threaded holes in the main part.

4.3 Waveguide

A WR-90 waveguide is used. The Waveguide Connector can be attached to the bottom of the main part. The waveguide is adapted to the connector with a WR-90 standard flange using M4 screws.

4.4 Frequency Tunability

The insertion of the sapphire rod is controlled by mounting the rod on top of a precision translation stage (MDE265 by Elliot Scientific) with 3 mm travel. The translation stage is mounted to a piece that is attached to the side of the QB cavity. It is possible to fix the translation stage in different positions, allowing a sapphire rod of 17 mm length to be inserted from 0 to 11 mm into the cavity.

4.5 Thermalisation

There are multiple M3 screw threads on each side. Screws secured in these threads which are connected to copper braids should allow for a better thermalisation of the aluminium blocks.

5 Experimental Results

For initial testing, only the fixed device is fabricated, see Fig. 13. Due to issues while manufacturing, the Waveguide Connector is not yet fabricated. Hence the complete system can not be measured. Instead, the connection to the waveguide is left open as a hole. This means that all cavity frequencies in the QB cavity differ from the values simulated above, due to the absence of the pin reaching into the QB cavity that connects to the waveguide.

In Fig. 14 a transmission measurement from input port 1 to output port 2 at the PF cavity is shown over a wide frequency range. Below 9 GHz the spectrum shows the following features: At f_{Readout} we observe a wide resonance, which is discussed below. At 7.9 GHz is a narrow resonance. This is the 102 mode of the PF cavity which couples weakly due to the finite size of the coupling pin. At higher frequencies, we observe a multitude of PF

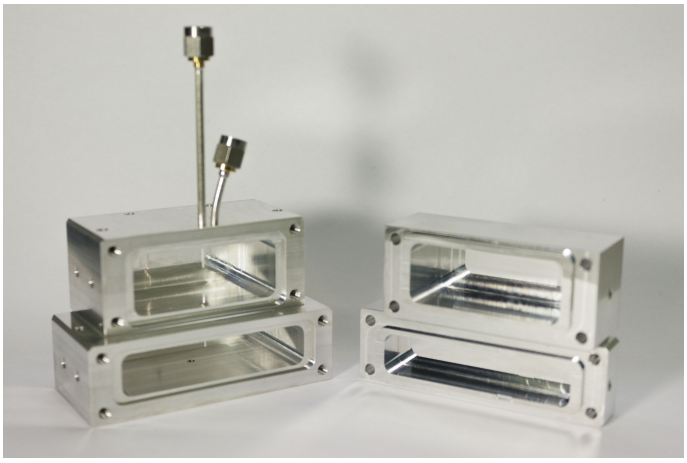

Figure 13: Photograph of the device used for the measurement. It features the following parts: Cavity Main to the left, PF Cavity Lid and QB Cavity Lid on top of each other to the right. The long straight coaxial cable is the output port, the short bent coaxial cable the input port. The left PF cavity shows the empty hole mount for the waveguide connection.

or QB cavity modes, making it hard to assign frequencies to specific modes (frequency crowding).

Fig. 15 shows the detailed spectrum around f_{Readout} of the transmission measurement. The S_{21}-parameter is fitted with a model for coupled cavity systems [11] in order to retrieve the coupling between the QB and PF cavity, analog to section 3.1.2. The resulting coupling strength is 8.4 MHz with the 101 mode of the PF cavity at 4.806 GHz and the QB at 4.883 GHz.

A simulation with the same setup gives a coupling of 11.3 MHz with the 101 mode of the PF cavity at 4.823 GHz and the QB at 4.890 GHz. The difference to the measured eigenfrequency is 17 MHz fo the PF and 7 MHz for the QB cavity.

5.1 Discussion of Experimental Results

The measured eigenfrequency of the 101 modes for both the QB and PF cavity differ from the simulation. The difference is above of what is expected from the manufacturing tolerances of the cavity dimensions. The reason for this is unclear. A precise measurement of the cavity dimensions is required to validate the fabricated pieces.

The measured coupling between the PF and QB cavity is close to the

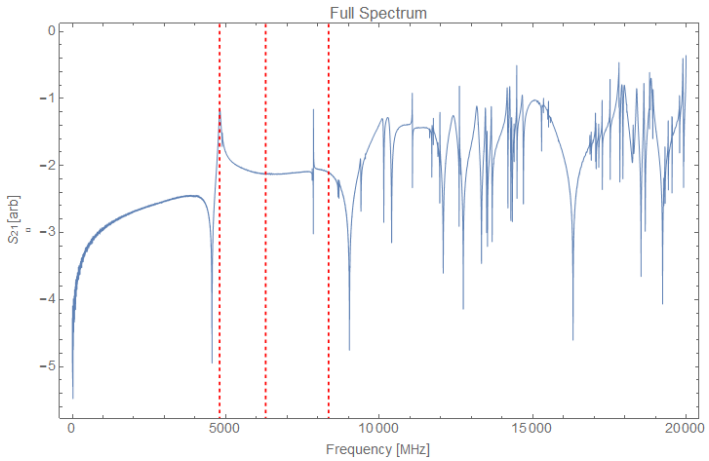

Figure 14: Measured absolute value of the S_{21}-Parameter. Port 1 is the input at the PF cavity, port 2 the output. The connection to the waveguide is left open as a hole. The red dotted vertical lines represent the three relevant frequencies: $f_{\text{Readout}} = 4.8$ GHz, $f_{\text{Qubit}} = 6.3$ GHz, $f_{\text{Transfer}} = 8.35$ GHz.

simulation. It is the first time that a coupling on the order of tens of MHz has been realized between 3D cavities. This demonstrates the feasibility of Purcell filters in 3D architectures.

The coupling of the QB cavity to the WR could not be measured. Since the experiment and the simulation agree for the coupling between the cavities and the coupling to the WR is similar, we expect it not to differ by much from the simulations. Thus the direct coupling form the QB cavity to the waveguide seems feasible.

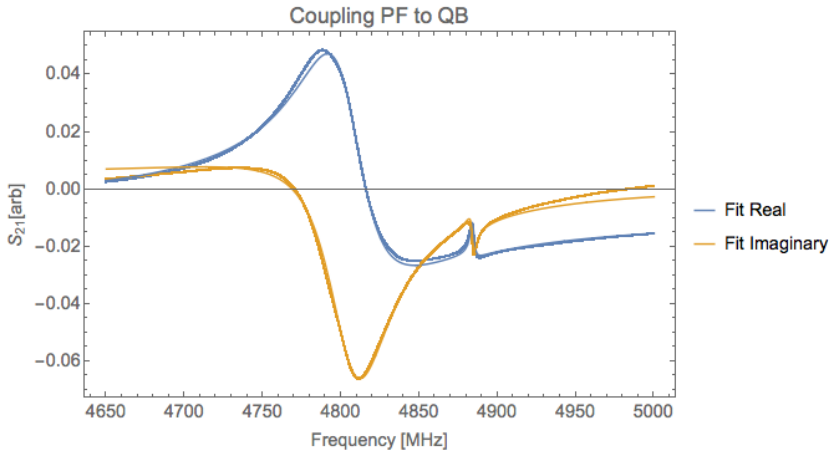

Figure 15: Real and imaginary part of measured S_{21}-Parameter (points), fitted with a complex Lorentzian (line). Port 1 is the input at the PF cavity, port 2 the output. The connection to the waveguide is left open as a hole.

References

[1] C. Axline, L. Burkhart, W. Pfaff, M. Zhang, K. Chou, P. Campagne-Ibarcq, P. Reinhold, L. Frunzio, S. Girvin, L. Jiang, *et al.*, "On-demand quantum state transfer and entanglement between remote microwave cavity memories," *arXiv preprint arXiv:1712.05832*, 2017.

[2] P. Campagne-Ibarcq, E. Zalys-Geller, A. Narla, S. Shankar, P. Reinhold, L. Burkhart, C. Axline, W. Pfaff, L. Frunzio, R. Schoelkopf, *et al.*, "Deterministic remote entanglement of superconducting circuits through microwave two-photon transitions," *arXiv preprint arXiv:1712.05854*, 2017.

[3] P. Kurpiers, P. Magnard, T. Walter, B. Royer, M. Pechal, J. Heinsoo, Y. Salathé, A. Akin, S. Storz, J.-C. Besse, *et al.*, "Deterministic quantum state transfer and generation of remote entanglement using microwave photons," *arXiv preprint arXiv:1712.08593*, 2017.

[4] T. Walter, P. Kurpiers, S. Gasparinetti, P. Magnard, A. Potocnik, Y. Salathé, M. Pechal, M. Mondal, M. Oppliger, C. Eichler, and A. Wallraff, "Rapid, high-fidelity, single-shot dispersive readout of superconducting qubits," *Phys. Rev. Applied*, vol. 7, p. 054020, 2017.

[5] B. Hensen, H. Bernien, A. E. Dreau, A. Reiserer, N. Kalb, M. S. Blok, J. Ruitenberg, R. F. L. Vermeulen, R. N. Schouten, C. Abellan, W. Amaya, V. Pruneri, M. W. Mitchell, M. Markham, D. J. Twitchen, D. Elkouss, S. Wehner, T. H. Taminiau, and R. Hanson, "Loophole-free bell inequality violation using electron spins separated by 1.3 kilometres," *Nature*, vol. 526, pp. 682–686, oct 2015.

[6] G. Carvacho, J. Carine, G. Saavedra, A. Cuevas, J. Fuenzalida, F. Toledo, M. Figueroa, A. Cabello, J.-A. Larsson, P. Mataloni, G. Lima, and G. B. Xavier, "Postselection-loophole-free bell test over an installed optical fiber network," *Phys. Rev. Lett.*, vol. 115, p. 030503, 2015.

[7] M. Giustina, M. A. M. Versteegh, S. Wengerowsky, J. Handsteiner, A. Hochrainer, K. Phelan, F. Steinlechner, J. Kofler, J. Larsson, C. Abellan, W. Amaya, V. Pruneri, M. W. Mitchell, J. Beyer, T. Gerrits, A. E. Lita, L. K. Shalm, S. W. Nam, T. Scheidl, R. Ursin, B. Wittmann, and A. Zeilinger, "A significant-loophole-free test of bell's theorem with entangled photons," *arXiv:1511.03190*, 2015.

[8] S. Zeytinoglu, M. Pechal, S. Berger, A. A. Abdumalikov Jr., A. Wallraff, and S. Filipp, "Microwave-induced amplitude- and phase-tunable qubit-resonator coupling in circuit quantum electrodynamics," *Phys. Rev. A*, vol. 91, p. 043846, 2015.

[9] M. Pechal, L. Huthmacher, C. Eichler, S. Zeytinoğlu, A. Abdumalikov Jr., S. Berger, A. Wallraff, and S. Filipp, "Microwave-controlled generation of shaped single photons in circuit quantum electrodynamics," *Phys. Rev. X*, vol. 4, p. 041010, 2014.

[10] P. Kurpiers, T. Walter, P. Magnard, Y. Salathe, and A. Wallraff, "Characterizing the attenuation of coaxial and rectangular microwave-frequency waveguides at cryogenic temperatures," *EPJ Quantum Technology*, vol. 4, no. 1, p. 8, 2017.

[11] E. A. Sete, J. M. Martinis, and A. N. Korotkov, "Quantum theory of a bandpass purcell filter for qubit readout," *Phys. Rev. A*, vol. 92, p. 012325, Jul 2015.

[12] A. Taflove, A. Oskooi, and S. G. Johnson, *Advances in FDTD computational electrodynamics: photonics and nanotechnology*. Artech House, 2013.

[13] S. E. Nigg, H. Paik, B. Vlastakis, G. Kirchmair, S. Shankar, L. Frunzio, M. H. Devoret, R. J. Schoelkopf, and S. M. Girvin, "Black-box superconducting circuit quantization," *Phys. Rev. Lett.*, vol. 108, p. 240502, Jun 2012.

[14] J. Fankhauser, "Frequency-tunable transmon qubit in a 3d copper cavity," Master's thesis, ETH Zurich, 2016.

A Qubit Lifetime Simulation

The qubit lifetime is a crucial parameter, especially regarding quantum computing. However, it can often only be measured from an existing setup, but not simulated beforehand.

In the following, some thoughts and attempts to simulate qubit lifetimes are discussed, which would make it possible to predict qubit lifetime during the design.

A.1 Theory

A.1.1 Approach A

Following Fermi's Golden Rule, the spontaneous emission rate is directly proportional to the local density of states (LDOS). The LDOS depends on the power exerted by a classical dipole, which depends on the electric field at the point of the dipole source, see [12] for a detailed derivation.

The LDOS is given by

$$LDOS(\vec{r}) = -\frac{2}{\pi}\epsilon(\vec{r})\frac{Re[\vec{E}(\vec{r})\cdot\vec{p_0}]}{|\vec{p_0}|^2}, \tag{4}$$

where $\epsilon(\vec{r})$ is the permittivity, $\vec{E}(\vec{r})$ the electric field at position $\vec{r}$ and $\vec{p_0}$ the (real) electric dipole moment.

The spontaneous emission rate is then

$$\Gamma = \frac{\pi\omega}{3\hbar\epsilon_0}|\vec{\hat{p}}|^2 LDOS(\vec{r}_D), \tag{5}$$

with ω the frequency, $\vec{\hat{p}}$ the quantum dipole operator and $\vec{r_D}$ the position of the dipole.

Using the semi-classical approximation $|\vec{\hat{p}}|^2 \approx |\vec{p_0}|^2$, plugging in the LDOS and assuming vacuum permittivity:

$$\Gamma \approx -\frac{2\omega}{3\hbar}Re[\vec{E}(\vec{r_D})\cdot\vec{p_0}], \tag{6}$$

A.1.2 Approach B

This approach closely follows [13]. The main idea is to approximate the linear elements of a qubit in a 3D cavity with an equivalent electrical circuit. The qubit itself is not simulated, it is placed only afterwards in post-processing.

This is done by adding the qubit capacity C_j and inductivity L_j, which defines its transition frequency, to the simulated impedance at the qubit.

The resulting impedance $Z_{\mathrm{Sim}}(\omega)$ can be decomposed using Foster's theorem into parts corresponding to every resonance. From the parameters of this decomposition, the lifetime $T_1(\omega_p)$ of a specific mode p can be calculated. This is also valid for the qubit mode.

To get the lifetime for different qubit transition frequencies, i.e. $T_1(\omega)$, the impedance $L_j(\omega)$ is set frequency dependant, corresponding to the qubit transition frequency. Thus ω always represents the qubit mode now, and $T(\omega)$ is its lifetime.

This way we can tune our qubit to different transition frequencies and simulate its lifetime in our cavity at all these frequencies.

A.2 Simulation

For both approaches, we need to place and simulate a dipole inside our cavity. We use COMSOL Multiphysics 5.1 for this purpose. An example of such a model is shown in Fig. 16.

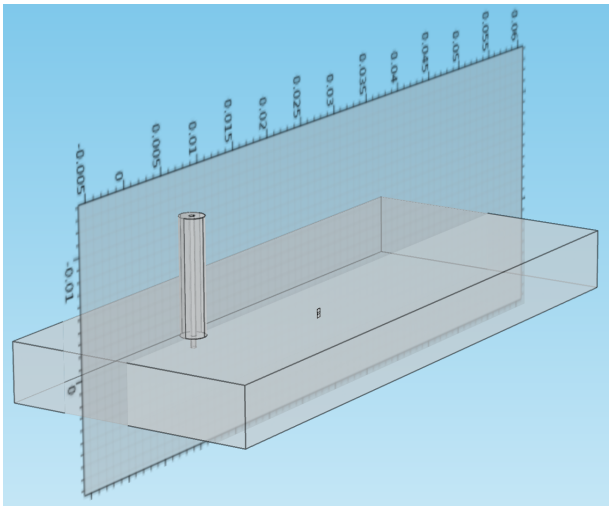

Figure 16: Example of a dipole inside a 3D cavity with one coaxial output port. The dipole is defined on a 2D work plane.

The dipole is best modelled by placing two rectangular pads in a 2D work plane, as seen in Fig. 17. The thickness of the pads is neglected, but the simulation runs much faster due to a more efficient meshing.

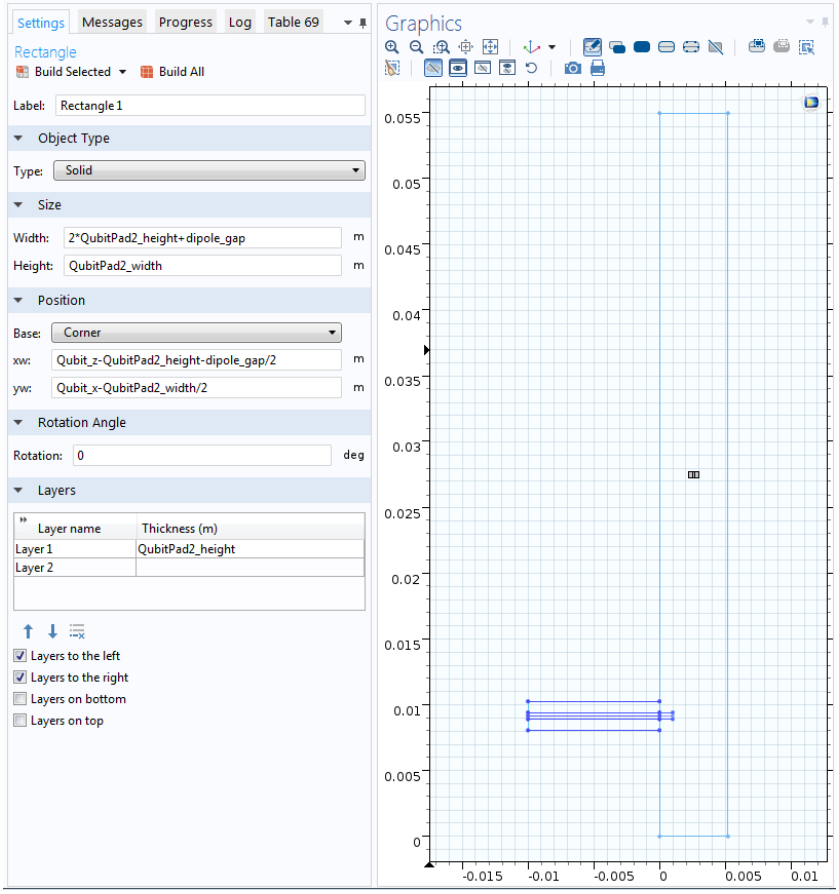

Figure 17: Definition of rectangular dipole pads (left) and view of the 2D work plane (right) in COMSOL.

In order to make the dipole pads conductive, a new Perfect Electric Conductor (PEC) boundary condition has to be created, see Fig. 18 and 19. The dipole can not be selected when using the initial PEC.

The dipole is completed by defining an lumped port as an input, as seen in Fig. 20. From this port, the dipole can be excited and the impedance can evaluated ("emw.Zport").

A.3 Conclusion

Unfortunately, we did not get satisfactory results. Following approach B, Fig. 21 shows the simulated qubit lifetime for the 3D cavity in [14]. In this

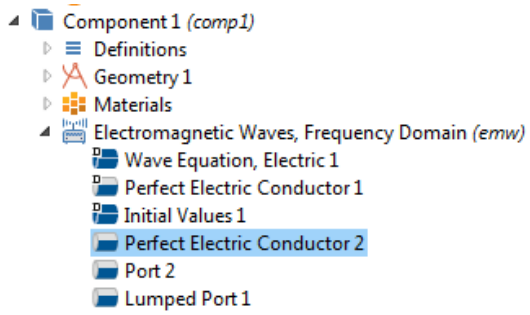

Figure 18: Initial PEC 1 used for defining the 3D cavity and new PEC 2 used for the dipole.

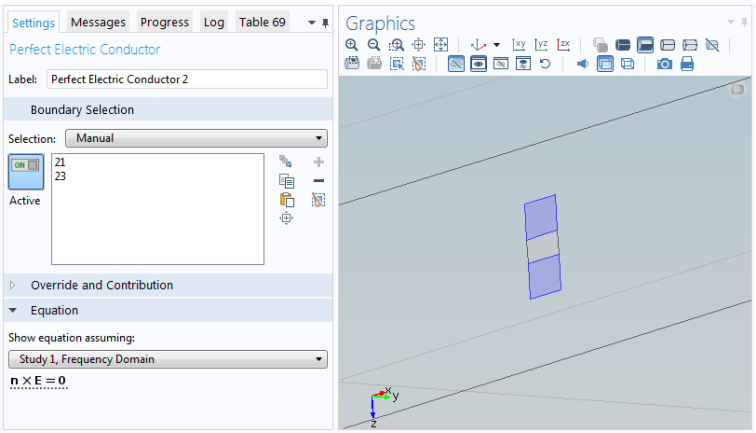

Figure 19: Perfect Electric Conductor boundary condition applied to the two dipole pads.

cavity design, the first two modes the qubit couples to are the 101 mode at 7.1 GHz and the 103 mode at 10.5 GHz. The qubit does not couple to the 102 mode at 8.6 GHz. Near resonance of the 101 and 103 modes, the simulation agrees well with the Purcell formula and shows a reduced qubit lifetime. However off-resonance, where we expect longer qubit lifetimes, the simulated lifetime is too short, below the limit imposed by the Purcell effect. As expected, the simulated lifetime is not further reduced due to the 102 mode at 8.6 GHz.

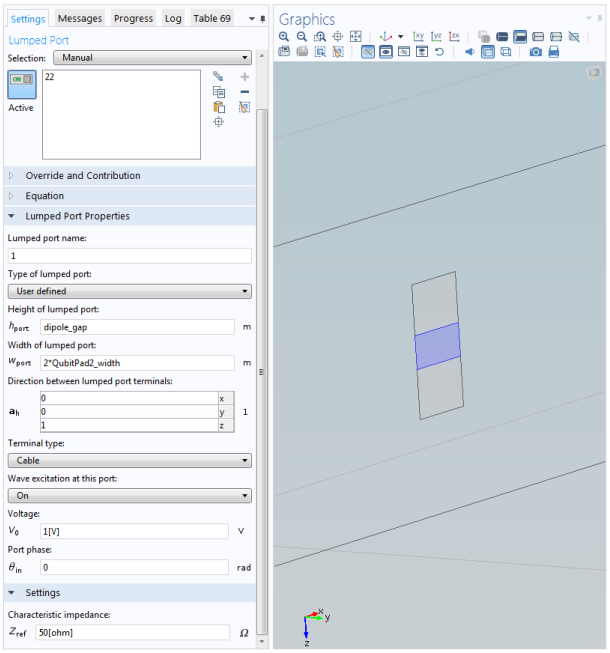

Figure 20: Lumped Port (input) defined between the dipole pads.

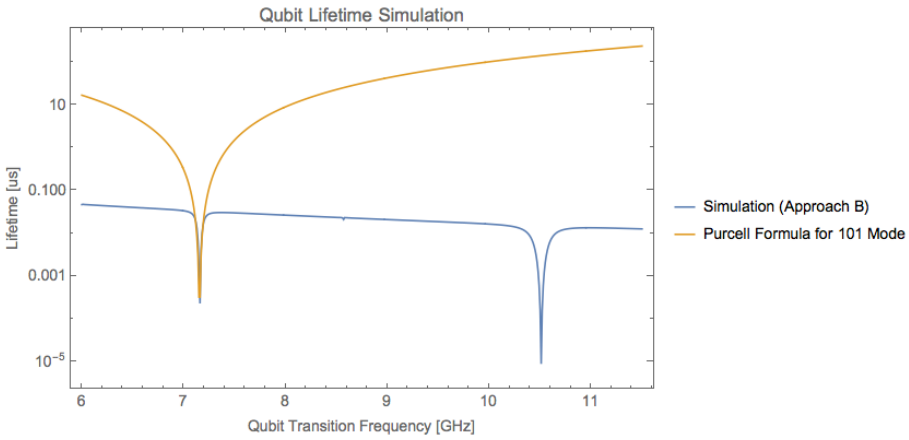

Figure 21: Simulation of the qubit lifetime following approach B. The Purcell formula is plotted for the 101 mode.

B Technical Drawings

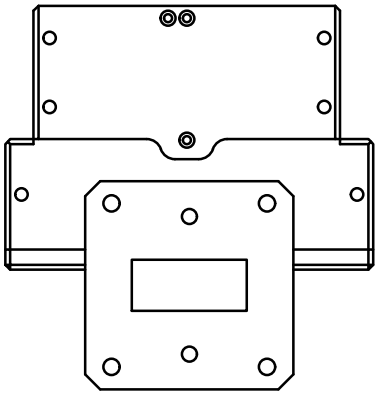

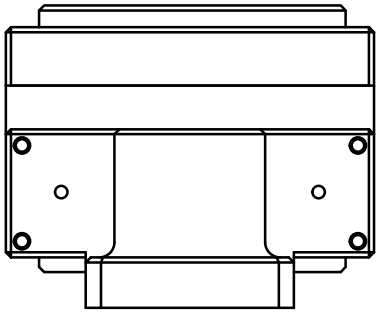

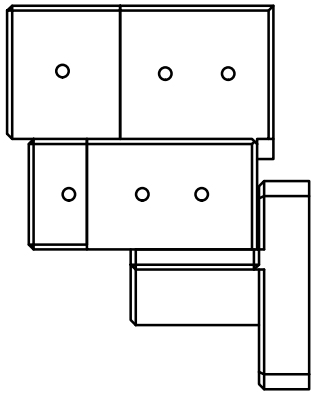

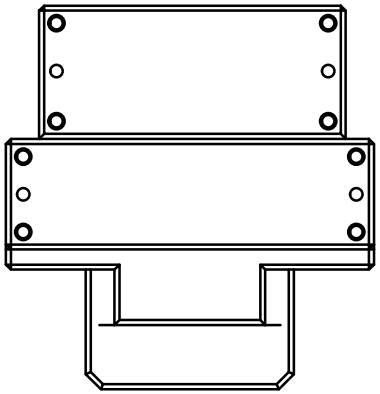

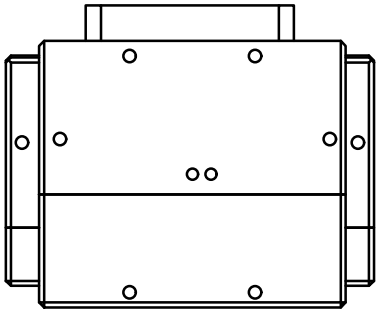

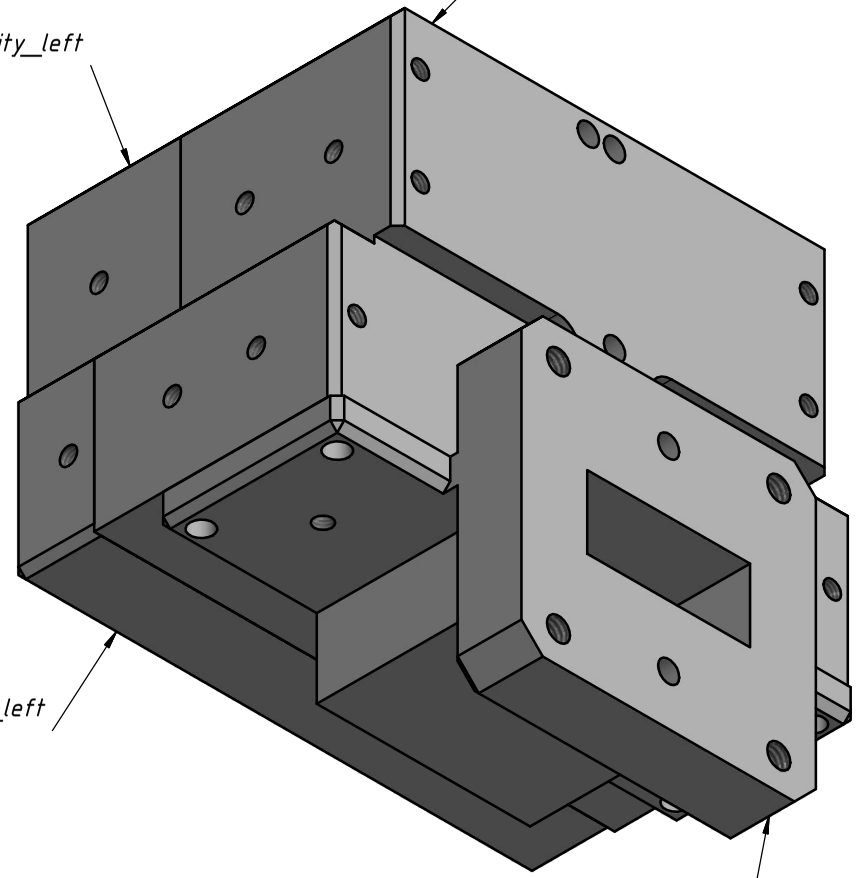

General Tolerances	Linear Dimensions							Angular Dimensions					
Dimensions in [mm] ISO-2768-mH	>0.5 to 6	> 6 to 30	>30 to 120	>120 to 400	>400 to 1000	>1000 to 2000	>2000 to 4000	to 10	> 10 to 50	>50 to 120	>120 to 400	>400	
	±0.1	±0.2	±0.3	±0.5	±0.8	±1.2	±2	±1°	±0°30'	±0°20'	±0°10'	±0°5'	

Material	Weight	Quantity	Cost center		Designed	05.10.2017	Nick Schwegler
	N/A		Phone nr.	+41 44 633 31 16	Checked		

Rev.	Description	Date	Name
		06.11.2015	Melvin Frey

ETH ZÜRICH
QUANTUM DEVICE LAB

Projekt

Part: 3D_cavity_model_Option2v6.iam

Description

1:1 | A3 | Page 1 of 1

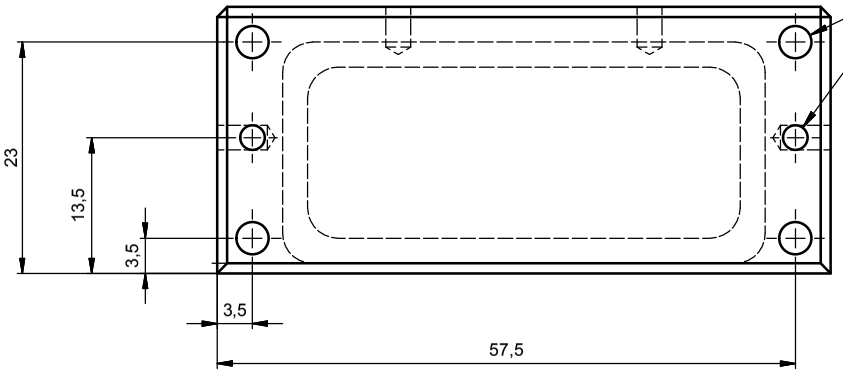

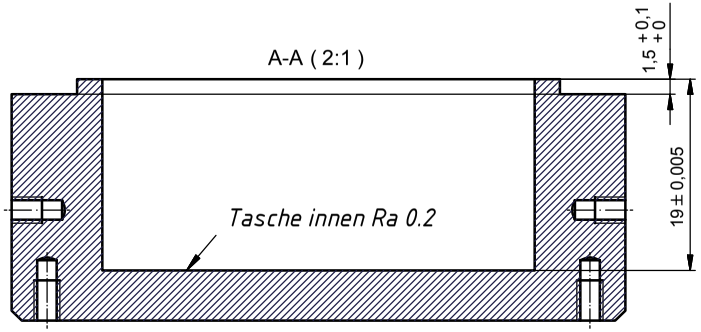

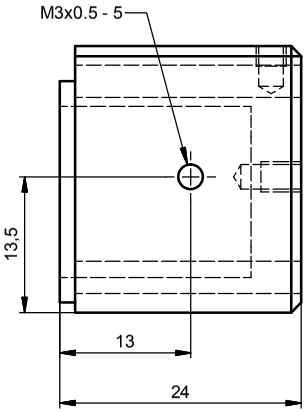

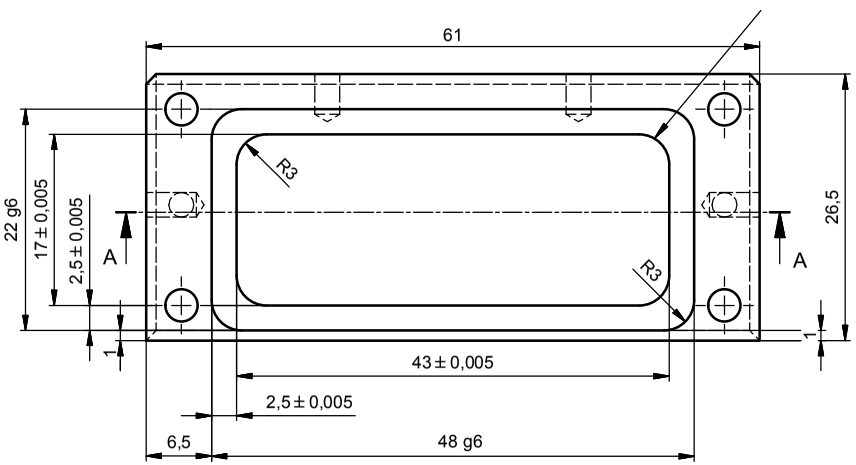

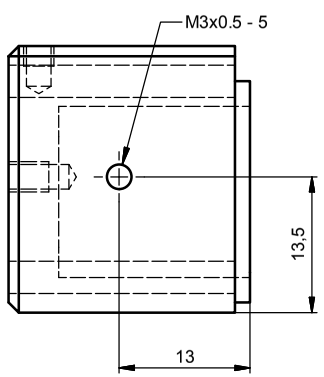

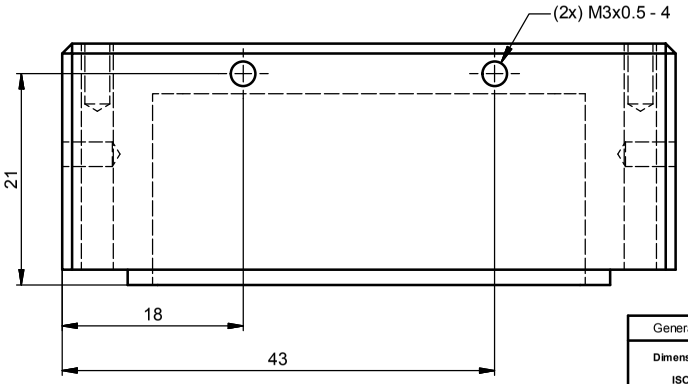

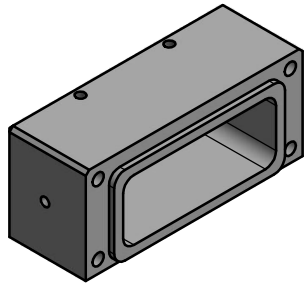

EN AW 1050 A

General Tolerances	Linear Dimensions							Angular Dimensions					
Dimensions in [mm] ISO-2768-mH	>0.5 to 6	> 6 to 30	>30 to 120	>120 to 400	>400 to 1000	>1000 to 2000	>2000 to 4000	to 10	>10 to 50	>50 to 120	>120 to 400	>400	
	±0.1	±0.2	±0.3	±0.5	±0.8	±1.2	±2	±1°	±0°30'	±0°20'	±0°10'	±0°5'	

Ra 1.6 (√)

Part: PF_Cavity_left.ipt

Description:

Material	Weight	Quantity	Cost center		Designed	06.10.2017	Nick Schwegler
Generic	N/A		Phone nr.	+41 44 633 31 16	Checked		

Rev.	Description	Date	Name
		06.11.2015	Melvin Frey

ETH ZÜRICH
QUANTUM DEVICE LAB

Projekt

2:1 | A3 | Page 1 of 1

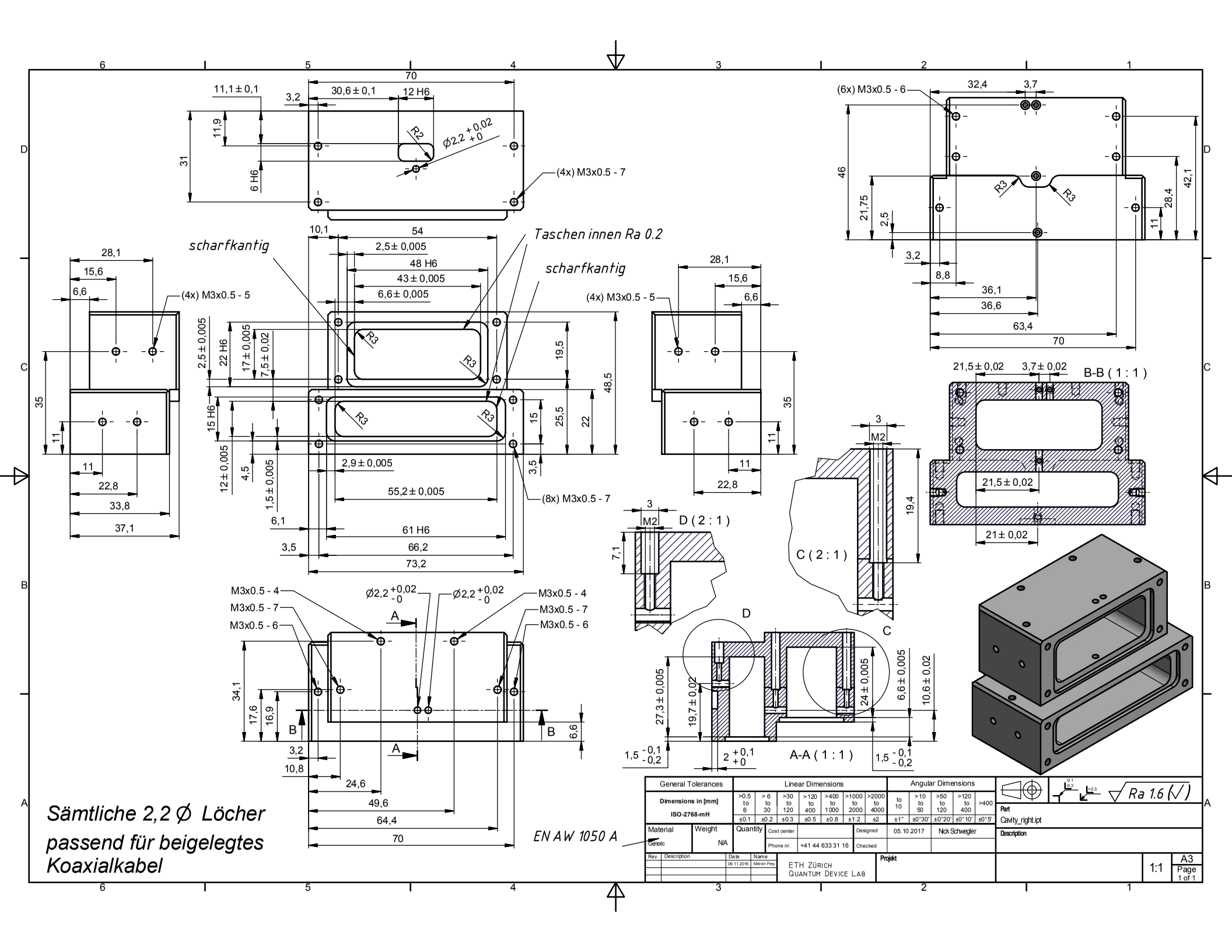
scharfkantig
Taschen innen Ra 0.2
scharfkantig
(4x) M3x0.5 - 5
(4x) M3x0.5 - 7
(8x) M3x0.5 - 7
(6x) M3x0.5 - 6
B-B (1 : 1)
D (2 : 1)
C (2 : 1)
A-A (1 : 1)
EN AW 1050 A
Ra 1.6
Sämtliche 2,2 Ø Löcher
passend für beigelegtes
Koaxialkabel
General Tolerances
Dimensions in [mm]
ISO-2768-mH
Linear Dimensions
Angular Dimensions
Material
Generic
Weight
N/A
Quantity
Cost center
Phone nr.
+41 44 633 31 16
Designed
05.10.2017
Nick Schwegler
Checked
Part
Cavity_right.ipt
Description
Rev.
Description
Date
Name
06.11.2015
Melvin Frey
ETH ZÜRICH
QUANTUM DEVICE LAB
Projekt
1:1
A3
Page
1 of 1

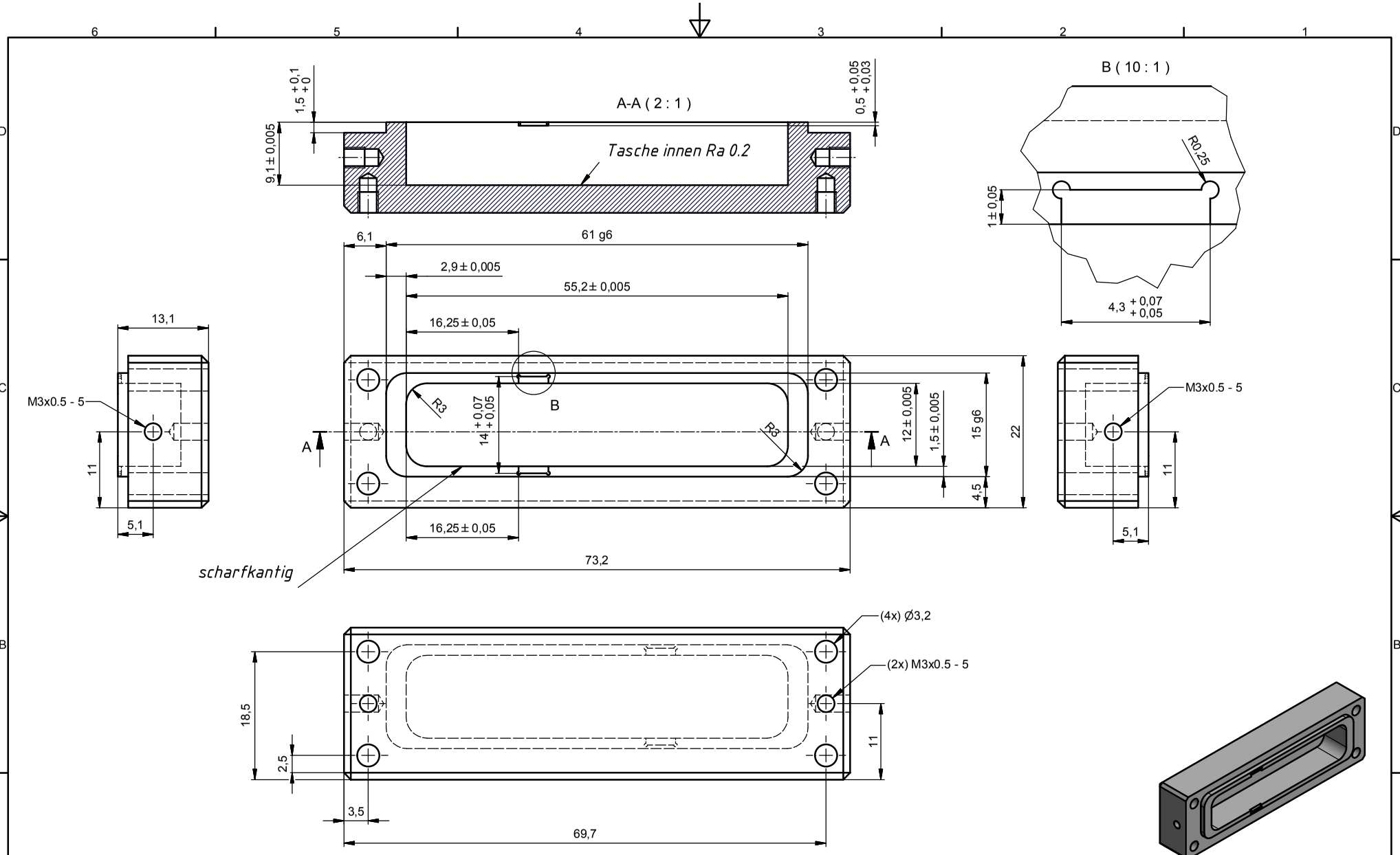

EN AW 1050 A

General Tolerances	Linear Dimensions							Angular Dimensions					
Dimensions in [mm] ISO-2768-mH	>0.5 to 6	> 6 to 30	>30 to 120	>120 to 400	>400 to 1000	>1000 to 2000	>2000 to 4000	to 10	>10 to 50	>50 to 120	>120 to 400	>400
	±0.1	±0.2	±0.3	±0.5	±0.8	±1.2	±2	±1°	±0°30'	±0°20'	±0°10'	±0°5'

Ra 1.6 (√)

Material	Weight	Quantity	Cost center		Designed	06.10.2017	Nick Schwegler
Generic	N/A		Phone nr.	+41 44 633 31 16	Checked		

Part: QB_Cavity_left.ipt

Description:

Rev.	Description	Date	Name
		06.11.2015	Melvin Frey

ETH ZÜRICH
QUANTUM DEVICE LAB

Projekt:

2:1 | A3 | Page 1 of 1

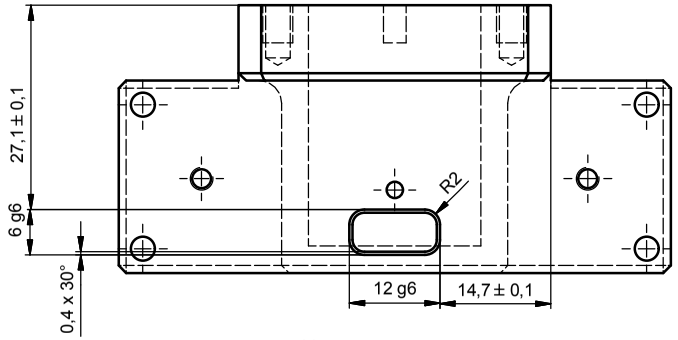

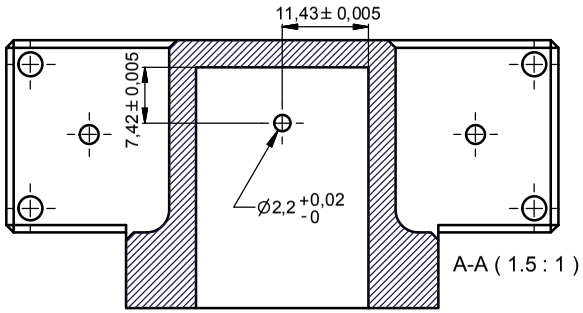

2,2 Ø Loch passend für beigelegtes Koaxialkabel

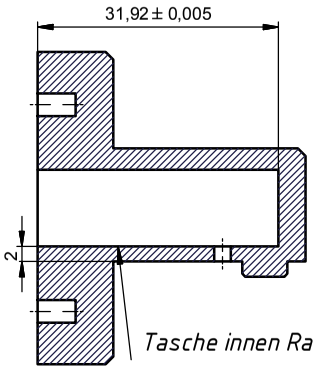

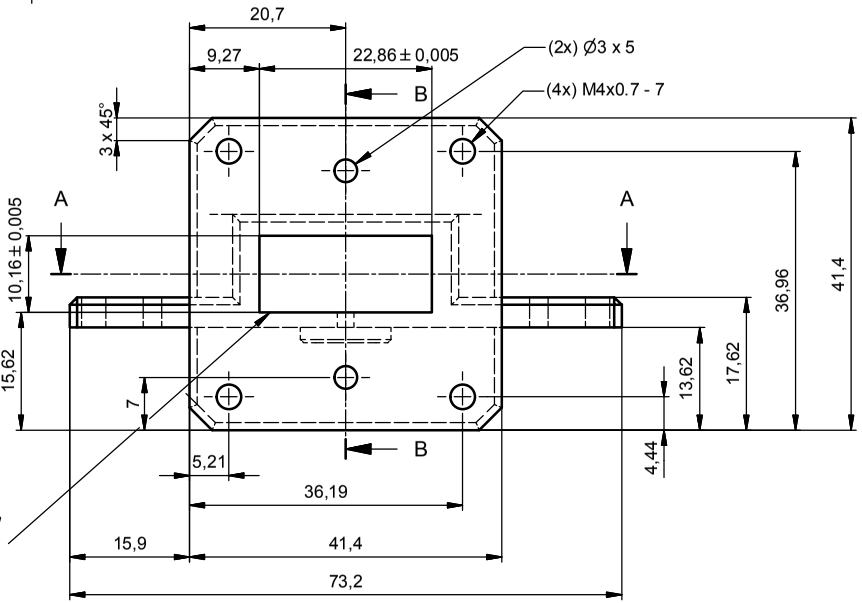

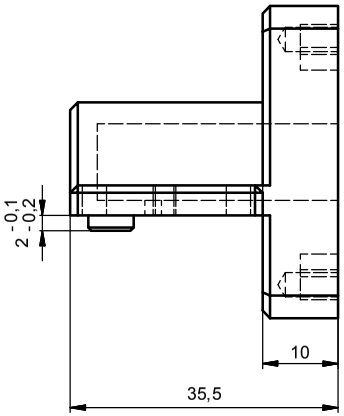

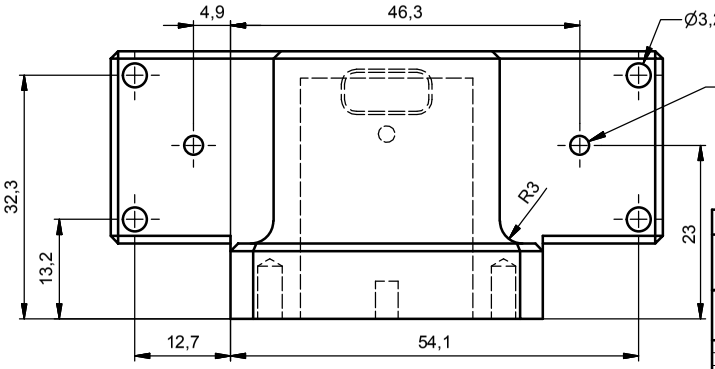

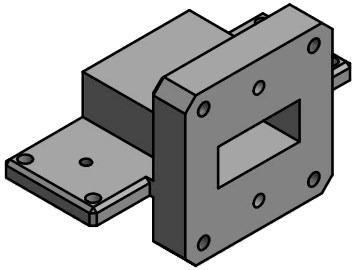

EN AW 1050 A

General Tolerances	Linear Dimensions							Angular Dimensions					Ra 1.6 (√)
Dimensions in [mm] ISO 2768-mH	>0.5 to 6	> 6 to 30	>30 to 120	>120 to 400	>400 to 1000	>1000 to 2000	>2000 to 4000	to 10	>10 to 50	>50 to 120	>120 to 400	>400	Part: Waveguide_connector.ipt
	±0.1	±0.2	±0.3	±0.5	±0.8	±1.2	±2	±1°	±0°30'	±0°20'	±0°10'	±0°5'	Description

Material	Weight	Quantity	Cost center		Designed	06.10.2017	Nick Schwegler
Generic	N/A		Phone nr.	+41 44 633 31 16	Checked		

Rev.	Description	Date	Name
		06.11.2015	Melvin Frey

ETH ZÜRICH
QUANTUM DEVICE LAB

Projekt

1.5:1 | A3 | Page 1 of 1

Eidgenössische Technische Hochschule Zürich
Swiss Federal Institute of Technology Zurich

Declaration of originality

The signed declaration of originality is a component of every semester paper, Bachelor's thesis, Master's thesis and any other degree paper undertaken during the course of studies, including the respective electronic versions.

Lecturers may also require a declaration of originality for other written papers compiled for their courses.

I hereby confirm that I am the sole author of the written work here enclosed and that I have compiled it in my own words. Parts excepted are corrections of form and content by the supervisor.

Title of work (in block letters):

Design and Characterization of a 3D Superconducting Architecture for Fast Readout and Remote Entanglement

Authored by (in block letters):

For papers written by groups the names of all authors are required.

Name(s):	**First name(s):**
Schwegler	Nick Timm

With my signature I confirm that

- I have committed none of the forms of plagiarism described in the 'Citation etiquette' information sheet.
- I have documented all methods, data and processes truthfully.
- I have not manipulated any data.
- I have mentioned all persons who were significant facilitators of the work.

I am aware that the work may be screened electronically for plagiarism.

Place, date	**Signature(s)**
Zurich, 08.04.2018	Nick Schwegler

For papers written by groups the names of all authors are required. Their signatures collectively guarantee the entire content of the written paper.